LM-07K020
March 27, 2007

Oxidative Dissolution of Nickel Metal in Hydrogenated Hydrothermal Solutions

SE Ziemniak, PA Guilmette, RA Turcotte, HM Tunison

Oxidative Dissolution of Nickel Metal in Hydrogenated Hydrothermal Solutions

S. E. Ziemniak*
P. A. Guilmette
R. A. Turcotte
H. M. Tunison

March 2007

Lockheed Martin Corporation
P. O. Box 1072
Schenectady, New York, 12301-1072

*Corresponding author. Tel.: +1-518-395-6887; fax: +1-518-395-7298
E-mail address: ziemnia@kapl.gov

ABSTRACT

A platinum-lined, flowing autoclave facility is used to investigate the solubility behavior of metallic nickel in hydrogenated ammonia and sodium hydroxide solutions between 175 and 315ºC. The solubility measurements were interpreted by means of an oxidative dissolution reaction followed by a sequence of Ni(II) ion hydrolysis reactions:

$$Ni(s) + 2H^{+}(aq) = Ni^{2+}(aq) + H_2(g)$$

and

$$Ni^{2+}(aq) + nH_2O = Ni(OH)_n^{\,2-n}(aq) + nH^{+}(aq)$$

where n = 1 and 2. Gibbs energies associated with these reaction equilibria were determined from a least-squares analysis of the data. The extracted thermochemical properties ($\Delta_f G^\circ$, $\Delta_f H^\circ$ and S°) for $Ni^{2+}(aq)$, $Ni(OH)^{+}(aq)$ and $Ni(OH)_2(aq)$ were found to be consistent with those determined in a previous solubility study of $NiO/Ni(OH)_2$ conducted in our laboratory. The thermodynamic basis of the Ni/NiO phase boundary in aqueous solutions is examined to show that Ni(s) is stable relative to NiO(s) in solutions saturated at 25ºC with 1 atm H_2 for temperatures below 309ºC.

KEY WORDS: nickel, nickel base alloys, aqueous solutions, hydrothermal solutions, nickel(II) ion hydrolysis, oxidation, corrosion, pressurized water reactors

BACKGROUND

Nickel base NiCrFe alloys are the preferred material for containing the reactor coolant in US commercial pressurized water reactors (PWRs), as well as in fabricating PWR steam generator tubing [1]. Although these materials have inherently lower corrosion rates than the iron base FeCrNi alloys used in other PWRs throughout the world, and thereby experience less severe problems with transported corrosion products, two other issues must be dealt with: (1) increased radiological consequences of activation of transported ^{58}Ni to ^{58}Co and (2) stress corrosion cracking (SCC). The latter has been especially costly for the French nuclear power industry; having to prematurely replace all of its Alloy 600-tubed steam generators with Alloy 690 units [2].

Previously, we reported the results of solubility testing conducted with NiO (bunsenite) [3], which quantified the solution thermodynamics of this corrosion product of nickel base alloys and demonstrated the importance of temperature and pH in transporting soluble Ni(II) ionic species in hydrothermal solutions. These studies were conducted in deoxygenated waters blanketed with an atmosphere of nitrogen gas. Since PWR coolants also contain quantities of dissolved hydrogen to minimize radiolytic oxygen production, and recent SCC test results have concluded that a maximum SCC growth rate exists near the Ni/NiO phase boundary [4], our solubility test efforts were extended to include the effects of dissolved hydrogen on the solubility behavior of metallic nickel.

It is noteworthy that the corrosion of typical nickel base alloys (such as Alloy 600 or 690) in reactor coolant systems results in the formation of a mixed iron-nickel oxide of the spinel type: $(Ni_xFe_{1-x})Fe_2O_4$ [5]. On the basis of a thermodynamic analysis [5], it may be demonstrated that in such a mixed system, nickel(II) ion reduction to elemental nickel limits the maximum stoichiometry (x) achievable. Although x is a weak function of dissolved hydrogen level and

temperature, $x \approx 0.8$ for typical levels of H_2 at PWR temperatures. Under these conditions, the limiting Ni(II) ion solubility is also expected to equal that of the oxidative dissolution for nickel metal. That is, soluble levels of nickel ions in the reactor coolant are expected to be in equilibrium with a mixed iron-nickel spinel oxide of fixed stoichiometry and metallic nickel (rather than nickel(II) oxide).

EXPERIMENTAL

Materials

The solubility measurements were made using nickel metal shaped into dense spheres (~25 mesh; 0.7 mm) to minimize the generation of particulate material, which would interfere with the solubility measurements. This material was purchased from Sherrett-Gordon Mines. Digestion in concentrated HNO_3 followed by analysis by ICP-OES found cobalt (0.17%) to be the major impurity.

X-ray diffraction analysis, performed using copper K" radiation and a tungsten internal standard, confirmed the presence of a single phase (cubic lattice) with lattice parameter a_0 = 3.5247(1) Å. This value is in excellent agreement with that of metallic nickel, per PDF card 04-0850 (3.524 Å). As seen in Fig. 1 and confirmed by the broadened XRD peaks, significant amounts of plastic deformation are present in the surface of the Ni-spheres. None of these chemical and mechanical imperfections are expected to affect saturation solubility levels.

De-ionized, deoxygenated water was used throughout the experimental program. Absolutely pure water has been assigned a resistivity of 18.23 Mohm-cm at 25ºC. However, due to the presence of (metal) ion contaminants in most laboratory 'pure' water supply systems, this value may be significantly lower and remedial actions must be considered to assure sufficiency of water quality. For example, the presence of trace metals in the ion exchange resins used in

most common purification systems and in the piping used to deliver the water to its end use (i.e., as feedwater or ultrapure analytical water), metals such as nickel and iron are normally present in this water at the sub-ppb levels. The conventional water purification system that supplied our experimental apparatus relied on charcoal and ion exchange resin columns and delivered pure water from stainless steel storage tanks having a resistivity ≥10 Mohm-cm.

Feedwater quality was improved by Teflon-coating the feed tanks in the solubility apparatus and equipping them with a final-polish, mixed-bed ion exchange resin column known to have low metals leakage; recirculation was continued until the tank water achieved an electrical resistivity >17 Mohm-cm at 25ºC. Secondly, the ion exchange system for obtaining ultrapure, analytical water from the lab pure water supply system was upgraded by installing two different water purification systems: (a) a Spectrapure recirculating unit (Tempe AZ) and (b) an 'element' (single pass) system from Millipore. The Spectrapure system employed special, low metals content, mixed-bed resins (Diaion, manufactured by Mitsubishi), to provide ultrapure water used for the nickel analyses by inductively coupled plasma mass spectrometry (ICPMS). The resistivity of this water exceeded 18.2 Mohm-cm. The Millipore system also produced water with resistivity values exceeding 18.2 Mohm-cm and was also used to prepare the ICPMS standards. Both water purification systems provided water (acidified to 1% with ultrapure nitric acid) having background nickel concentrations between 15 and 30 ppt (0.25 to 0.50 nmol-kg^{-1}).

Commercial-grade hydrogen gas was used to sparge dissolved oxygen to values <0.005 mg-L^{-1}. Test solutions were prepared volumetrically in the feed tanks using ultrapure ammonium hydroxide, or in some cases, ultrapure sodium hydroxide (Labchem, 50 wgt/vol %).

Apparatus

The solubility measurements were made using the flowing autoclave arrangement shown in Fig. 2. The feed tanks, pump, filter holder, and tubing between the feed tanks and first autoclave were of stainless steel. The two test autoclaves were of stainless steel with platinum liners. The tubing, cooler, and valves (which comprised the sampling station) were of stainless steel, the tubing and cooler having platinum linings. The feed tanks, each having a 115-L capacity, were Teflon-lined and equipped with supplemental ion exchange capability to reduce contaminant input levels of nickel to <0.5 nmol-kg^{-1}. After filling with deoxygenated, deionized water, and deionizing, additions of solutions containing ultrapure chemicals were made to obtain the desired feedwater compositions. These compositions are listed in Table 1.

Hydrogen gas was bubbled through the feed solution and between one and four atmospheres of this gas was maintained over the feed solution during all tests. The hydrogen concentration in the feedwater was calculated to range between 790 and 3160 :mol-kg^{-1} on the basis of pressure in the feed tank and Henry's law coefficient for the solubility of hydrogen in water [6, 7]. Confirmatory hydrogen analyses of feedwater agreed to within 7% of those determined by application of Henry's law coefficient (17.7 scc-kg^{-1}-atm^{-1} at 25ºC) [6,7].

A Milton Roy piston-type pump supplied feedwater to the high-pressure system. A flow rate of (6.0 ± 0.5) cm^3-min^{-1} was maintained at room temperature. From the pump, the feedwater at ambient temperature passed through a high pressure filter holder containing a 0.2 :m Uni-Pore™ polycarbonate filter membrane. After the filter, the feed solution entered two platinum-lined autoclaves connected in series. Each autoclave had an internal volume of ~100 cm^3 (2.5 cm diam. x 20 cm length). The first autoclave was empty and acted as a solution preheater, whereas the second autoclave contained 522 g of nickel pellets. The spheres were confined to the test autoclave by means of a fine platinum screen at the inlet and a sintered, micrometallic,

disc-type filter at the outlet. To increase the hot filtering capacity of the frit, it had been compressed from an initial thickness of 2.45 to 1.65 mm.

The average contact time between the feed solution and bed was 4.7-6.2 min, depending on the temperature. Based on sampling results obtained during shakedown of heater and temperature control system upgrades, the above flow rate was sufficient to achieve saturation solubility values: flow reduction to 3 cm^3-min^{-1} yielded no increases in Ni(II) ion concentration.

After leaving the second autoclave, the test solution flowed immediately through a stainless steel cross, one leg of which was dead-ended and contained a platinum-sheathed thermocouple to monitor temperature of the exiting solution. The main leg directed the flow into the sampling line, while the remaining leg provided a secondary path through which the flow could be diverted in case the sampling line became plugged. This leg was also connected to a pressure gauge that monitored the system pressure.

The sampling system consisted of a water-jacketed cooler and a pressure regulating valve, located immediately upstream of the sample collection point. For safety purposes, a second valve (which always remained open) was installed between the cooler and pressure-regulating valve. All tubing between the two autoclaves and between the outlet of the second autoclave and sample collection point, including the cooler, were high-pressure Alloy 600 tubing lined with platinum. Both valves in the sampling system were fabricated from stainless steel and had titanium internals. During normal operation, the system pressure was maintained in the range 13.1-14.1 MPa.

Heat was supplied to the autoclaves by a Chromalox electrical heating element jacket, the temperature being controlled by a Modicon PID programmable logic controller (PLC). System

temperatures were monitored with iron-constanstan (J Type) thermocouples at three locations: (1) outer surfaces of the first and second autoclaves (four in parallel per autoclave, read as an average), (2) tubing at the entrance and outlet of the second autoclave, and (3) in the flow stream at the second autoclave outlet. The latter consisted of a small (0.025") diameter 'platinized' thermocouple that had been threaded into the top (outlet) of the test column to measure the actual test bed temperature. The liquid temperature at this location was unaffected by the subsequent heat losses experienced by the exiting solution in the sampling line. All thermocouples had been purchased with a stated "special error limit" of ±1.1 Cº; their outputs were also displayed on the PLC.

Operational and Analytical Procedures

Prior to the start of each test run, one of the feed tanks was prepared by rinsing, flushing, and filling with demineralized water. After chemical addition, the tank was sparged with hydrogen gas to facilitate mixing and to minimize oxygen. A blanket of hydrogen gas (1 – 4 atm; see Table I) was placed over the feed water upon completion of the sparging operation. The Ni bed was then flushed for a minimum of three days (at 260ºC), using a system flow rate of six cm^3-min^{-1}. The flushing period insured adequate time for equilibration with each new test chemistry. The sampling sequence, during which six samples were collected in acid-leached Nalgene bottles, was then initiated. After sampling, the PLC was set to establish a new temperature. Although 120-150 min were required to establish the new temperature, the system was allowed to stabilize at the new temperature for at least one day before the sampling procedure was repeated. With the exception of Run 4, all sampling sequences were conducted in an increasing/decreasing/increasing mode so that the 175-315ºC interval was completed in increments of 14 Cº. Run 4 was a double (replicabilty) run in which sampling was conducted in increments of 14 Cº; first in an increasing sequence (175 to 315ºC, Run 4U) and then in a decreasing sequence (315 to 175ºC, Run 4D).

Feed tank and system effluent samples were collected during each run and analyzed for pH, conductivity, and oxygen. Ammonia was determined by ion chromatography, while sodium hydroxide was determined by acid-base titration, using standardized hydrochloric acid solutions.

ICPMS Methodology

All Ni(II) ion concentrations measured in the present study were <0.5 ppb. Accurate analyses at such low levels required relatively large sample volumes (~30 cm^3) and the application of inductively coupled plasma mass spectrometry (ICPMS). An HP4500 Series 300 Inductively Coupled Plasma Mass Spectrometer manufactured by Hewlett-Packard was used for these analyses. Analytical accuracy is expected to be better than ±20% above the concentration of 0.2 $nmol\text{-}kg^{-1}$. The manufacturer's stated detection limit is 7 ppt Ni. To minimize adsorption on walls of the sample bottles, each sample was acidified to 0.5 or 1.0% nitric acid at least one day prior to analysis.

The successful application of ICPMS at nickel concentrations approaching this instrumental detection limit requires an ability to generate accurate instrumental calibration curves, which in turn, are generated using a source of nearly theoretically pure water. Presently, the 'standard addition' method was applied to develop the Ni calibration curves. A blank solution was prepared using ultrapure water and the desired concentration of 1% nitric acid solution; itself prepared from the ultrapure water supply and ultrapure nitric acid. Six aliquots of this solution were taken. All bottles (Nalgene) and equipment coming in contact with the standard solutions were acid-cleaned prior to use. The first aliquot was maintained as a blank. The other five aliquots were adjusted to nominal Ni concentrations of 100, 200, 500, 1000 and 1500-2000 ppt by adding known weights of a 2000 ppb Ni standard prepared in turn from a certified 1000 ppm Ni ICP standard. Table II shows typical calibration data. The instrument used linear regression

of these data to solve for the amount of nickel present in the blank solution. The instrument then automatically compensated for this nickel to generate a calibration curve that gave the true nickel concentration in any sample within the calibration range. This calibration curve passes through the origin (0 counts = 0 ppt).

For Ni concentrations within the range of the calibrated standards, i.e., 100-2000 ppt, the expected analytical accuracy is ±10%. Periodic checks were performed by analyzing several aliquots of a control standard with each sample set of unknowns. This concentration (of the control standard) ranged from 500-800 ppt, i.e., the mid-range of the calibration set, and the accuracy as determined by analysis of the control samples was within the above-stated accuracy.

The instrumental detection limit of 7 ppt Ni could not be demonstrated for the analytical standards used in the present test program because higher background levels of nickel were always present in the laboratory ultrapure water or nitric acid. The actual levels of nickel in the blank solution (1% nitric acid in ultrapure water) were found to vary between 15 and 30 ppt. In reality, the 7 ppt level may only be attainable by applying clean room technology. Since it is desired to only report values that are truly representative of the solubility experiments, and not from the support systems (i.e., pure water, sample tubes, etc.), a minimum reportable (mr) value concept was developed. A mr value was generated from the Ni levels found in the blank solutions. Analyses of a series of blank solutions will produce a mean and standard deviation about that mean; the same is true for a set of sample solutions. Since three standard deviations (sigma) correspond to a >95% confidence level of a normally distributed population about its mean, the mr valve for any sample is taken to be the mean value for the blank plus three standard deviations (for the blank). In this manner, the mr value provides confidence that any value larger than this value is a truly valid experimental data point. Therefore, series of 5-6

blank solutions were scattered throughout the analytical sequence to gauge instrumental variability and to develop the data needed to determine the mr value for each particular set of samples. Depending on the spread of these data on any one day, the mr value for nickel could be as high as 45-50 ppt for a set of unknowns.

RESULTS

Solubility Measurements/Reactions

Results from the experimental program, in terms of measured nickel solubilities as a function of temperature, are presented in Table III. The elemental nickel concentrations represent averages of six samples and are given in nanomolality units (i.e., 10^{-9} mol nickel per kilogram of water). The small amounts of material lost in the sampling line have been neglected. The temperature value listed for a particular sample was the test column effluent thermocouple reading after sampling was completed. Total measured nickel solubilities ranged between 0.4 and 400 nmol-kg^{-1}. (1 nmol-kg^{-1} = 58.7 ppt)

Given the hydrothermal environment in which metallic nickel was exposed, dissolution is expected to occur via the oxidation reaction

$$Ni(s) + 2H^{+}(aq) = Ni^{2+}(aq) + H_2(g) \quad (1)$$

followed by sequential Ni(II) ion hydrolysis reactions

$$Ni^{+2}(aq) + nH_2O = Ni(OH)_n^{2-n}(aq) + nH^{+}(aq) \quad (2)$$

and amminocomplexing reactions

$$Ni(OH)_n^{2-n}(aq) + NH_3(aq) = Ni(OH)_n(NH_3)^{2-n}(aq) \quad (3)$$

where n = 0, 1 and 2.

By expressing the concentration of each possible Ni(II) ion complex in terms of an (unknown) equilibrium constant and calculable H^+ ion and undissociated NH_3 concentrations, and equivalent pressures of dissolved hydrogen, the measured Ni(II) ion solubilities were separated into contributions from each of the individual complexes. The total molality of nickel in solution (i.e., saturation solubility limit) was then calculable by summation over all mononuclear Ni(II) ion species present. The unknown equilibrium constants were ultimately obtained by a regression analysis which minimized the differences between measured and calculated Ni(II) ion solubilities.

pH Determination

Evaluation of the experimental solubilities of Table III in terms of concentrations of the possible hydrolyzed/complexed Ni(II) species present required that the pH (hydronium ion concentration) be known at the existing solution conditions. This quantity depended on the molality of the alkaline reagent dissolved in solution (i.e., ammonia or sodium hydroxide), as well as its ionization constant and that of H_2O. The latter parameters, which are functions of solution temperature, are defined below in terms of thermodynamic activities ( ) and tabulated in Table IV.

$$K_W = (H^+)(OH^-) \quad (4)$$

$$K_B = (NH_4^+)(OH^-)/(NH_3) \quad (5)$$

with

$$\log K = b_1/T + b_2 + b_3 \ln T + b_4 T + b_5/T^2 \quad (6)$$

Both, K_W and K_B were pressure corrected (to 13.1 MPa), as well as ionic strength corrected, using the correlations presented in Refs. [8, 9].

In addition, the equivalent pressure of hydrogen dissolved in water at 25ºC (P_o, atm; per Table I) was calculated as a function of temperature by application of Henry's law; i.e., $P_{H2}(T) = [h(T)/h_o]P_o$. For thermodynamic consistency, values for Henry's law constant, $h(T)$, were calculated using the data of Gilpatrick and Stone [6] fitted to Eq. (6) with log K replaced by log h (atm per mol fraction).

Equilibrium constants for Eqs. (1)-(3) were corrected for small deviations from ideal solution behavior, by distinguishing between ionic concentration (i.e., molality) and thermodynamic activity

$$(a_i) = \gamma_i [m_i] \quad (7)$$

where (a_i) is the thermodynamic activity, γ_i is the ionic activity coefficient and $[m_i]$ is the ionic concentration. Because solution ionic strengths never exceeded 2 x 10^{-4}, ionic activity could be related to ionic strength by an extended Debye-Huckel expression [10]

$$\log \gamma_i = -S z_i^2 \sqrt{I} /(1+1.5\sqrt{I}) \quad (8)$$

where S is the temperature-dependent [11], limiting Debye-Huckel slope (0.51005 at 298 K), z_i

is the ionic charge number and *I* is the ionic strength (= ½ $\sum m_i z_i^2$).

An overall electroneutrality balance was finally applied to determine $[H^+]$ for each data point. In ammonium hydroxide solutions, the balance is

$$\sum_{n=0}^{3}(2-n)[Ni(OH)_n^{(2-n)+}]+\sum_{m=0}^{3}(2-n)[Ni(OH)_m(NH_3)^{(2-m)+}]+[NH_4^+]+[H^+]=[OH^-] \qquad (9)$$

The relatively low ammonia concentrations, together with existing information on multiple ammonia-complexing equilibria [12] indicate that multiple ammonia complex concentrations are expected to be low and have a negligible impact on pH. Hence the added complexity introduced by their inclusion in the neutrality balance is not justified.

Since all terms were expressible in terms of temperature and total dissolved ammonia concentrations, Eq. (9) was reduced to an algebraic equation in terms of the remaining unknown, $[H^+]$. To determine how a given scheme of Ni(II) complexes in solution could fit the results, a set of thermodynamic constants was substituted into the neutrality balance, and $[H^+]$ concentrations were calculated by a Newton-Raphson iteration procedure. These $[H^+]$ values were then used to compute all the soluble nickel species that, after being summed, could be compared with the measured Ni solubilities. The differences were then minimized via a generalized, nonlinear, least-squares curve-fitting routine based on Marquardt's algorithm [13].

When the solubility data were analyzed, the importance of relative errors (i.e., percentage errors), rather than absolute errors was accounted for by minimizing differences between the logarithms of the experimental and the predicted solubilities. The thermodynamic functions obtained were then resubstituted into the neutrality balance, and the two-step process was

repeated. Convergence (i.e., the condition when the calculated thermodynamic functions ceased to change) was attained after a single cycle because the dissolved metal ion concentrations were very low and had nearly negligible influences on changes in solution pH (i.e., <0.001 pH unit).

Thermodynamic Analysis

Equilibrium constants for the nickel dissolution and Ni(II) complexing reactions, Eqs. (1) – (3), were quantified via the thermodynamic relationships

$$-RT \ln K = \Delta G^{o} = \Delta H^{o} - T\Delta S^{o} \qquad (10)$$

which permitted calculation of all Ni(II) ion complex concentrations as functions of temperature using two parameters (ΔH^{o} and ΔS^{o}). This approximation is expected to be sufficient relative to a three parameter $\Delta G^{o}(T)$ model because Eqs. (1) – (3) are written in isocoulombic form [14]. Although equilibrium constants may be affected by pressure at T ≥275ºC (and correlated to water density), this expected effect is small at our test temperatures (T ≤315ºC) and was neglected in our analysis.

Due to the characteristic hydrolytic behavior of the Ni(II) aquoion and the alkaline pH range of the present study, many Ni(II) solubilities were <mr-values. This result, when coupled with a truncated temperature range, made it prudent to constrain the fit for the equilibrium involving the neutral $Ni(OH)_2(aq)$ hydroxocomplex (i.e., the least soluble species) to the $\Delta G^{o}(298)$ value based on standard free energies of formation for the Ni(II) aquoion and its hydroxocomplexes obtained during our previous NiO solubility study [3]. Results of the data-fitting procedure are shown in Figs. 3 and 4. In this manner, statistically significant fits were obtained for the thermodynamic functions of the unhydrolyzed $Ni^{2+}(aq)$ ion and two of its hydrolytic products:

$Ni(OH)^+(aq)$ and $Ni(OH)_2(aq)$. Contributions from the Ni(II) ion amminocomplexes, indicated by Eqs. (3), were not statistically significant.

Table V presents the fitted thermochemical parameters for the three nickel metal oxidative dissolution reactions. These fits resulted in an overall standard deviation between measured and fitted nickel solubilities of ±27% for a database consisting of 80 entries.

DISCUSSION OF RESULTS

Free Energy Changes for Oxidative Dissolution Reaction of Metallic Nickel

The fitted temperature dependence of the change in Gibbs energy for Eq. (1) is plotted in Fig. 5. Based on tabulated thermochemical properties for the chemical entities that comprise Eq. (1) [3, 15], a three-parameter (constant heat capacity) model was constructed to estimate the temperature dependence for Eq. (1) as

$$\Delta G°(T),\ \text{J mol}^{-1} = -38458 - 286.358\ T + 46.83\ T\ln T \qquad (11)$$

Figure 5 shows that the fitted and predicted Gibbs energies differ by <1 kJ mol^{-1} throughout the temperature range of the measurements (450 to 590 K). This degree of agreement is considered to be excellent and indicates that thermodynamic consistency exists between the present metallic nickel solubility measurements and our previous NiO solubility measurements [3].

Nickel(II) Ion Hydrolytic Equilibria

Subtraction of the Eq. (1) equilibrium from those determined for the two remaining reactions in Table V (i.e., those involving the $Ni(OH)^+(aq)$ and $Ni(OH)_2(aq)$ species) allowed Gibbs energies to be obtained for the Ni(II) ion hydrolysis reactions

$$Ni^{2+}(aq) + H_2O = Ni(OH)^+(aq) + H^+(aq) \qquad (12)$$

$$\Delta G°(T),\ \text{J mol}^{-1} = 22675 + 76.67\ T \qquad (13)$$

and $$Ni^{2+}(aq) + 2H_2O = Ni(OH)_2(aq) + 2H^+(aq) \quad (14)$$

$$\Delta G°(T),\ J\ mol^{-1} = 132259 + 9.46\ T \quad (15)$$

The Gibbs energies, Eqs. (13, 15), are plotted in Fig. 6 and compared with literature values based on our previous solubility measurements of NiO [3, 15]. Again, the agreement is excellent; the maximum deviations for $\Delta G°$ are <5 kJ mol^{-1} for Eq. (12) and <7.5 kJ mol^{-1} for Eq. (14).

Table VI summarizes the thermochemical properties obtained for the aqueous Ni(II) ion and its hydroxocomplexes and compares them with those derived from the three previous solubility studies conducted with $NiO/Ni(OH)_2$: Ziemniak and Goyette [3], Palmer *et al*. [15] and Tremaine and LeBlanc [16]. It is seen that the results obtained in our laboratory are internally consistent, i.e., the properties for $Ni^{2+}(aq)$ and $Ni(OH)_2(aq)$ deviate by less than the combined uncertainties of the measured values; the somewhat poorer agreement for the properties of $Ni(OH)^+(aq)$ may be caused by neglect of amminocomplexing in the present analysis. The inability of Refs. [15, 16] to obtain accurate properties for $Ni(OH)^+(aq)$ is explained by the narrow pH range over which this hydrolytic species is significant: our measurements emphasized this interval, while the others did not. The poorer agreement for the $Ni^{2+}(aq)$ properties demonstrated by Palmer *et al*. [15] may be an overcompensation for exclusion of the $Ni(OH)^+(aq)$ species.

Ni/NiO Phase Boundary

The equilibrium for the chemical reaction that defines the Ni/NiO phase boundary in aqueous solutions

$$Ni(s) + H_2O = NiO(s) + H_2(g) \quad (16)$$

may be written as

$$K_{eq} = P_{H2} \quad (17)$$

where P_{H2} is the partial pressure of hydrogen gas in equilibrium with the aqueous phase. It follows from Eq. (10) that changes in a third thermochemical property, namely heat capacity, may be included to provide a more accurate expression for ΔG° (hence K_{eq}):

$$\Delta G^{\circ}(T) = A - BT - CT\ln T \qquad (18)$$

where $A = \Delta H^{\circ}(298) - 298.15\ \Delta C_P{}^{\circ}(298)$

$B = \Delta S^{\circ}(298) - [1 + \ln(298.15)]\ \Delta C_P{}^{\circ}(298)$

$C = \Delta C_P{}^{\circ}(298)$

Based on values extracted from thermodynamic compilations [3, 15], it is found that $\Delta G^{\circ}(298)$ = 26.04 kJ-mol^{-1}, $\Delta H^{\circ}(298)$ = 46.53 kJ-mol^{-1}, $\Delta S^{\circ}(298)$ = 68.72 J-mol^{-1}-K^{-1} and $\Delta C_P{}^{\circ}(298)$ = -28.03 J-mol^{-1}-K^{-1} for Eq. (16), whereupon

$$\Delta G^{\circ}(T),\ \text{J-mol}^{-1} = 54887 - 256.45T + 28.03T\ln T \qquad (19)$$

The above equation indicates that an aqueous solution saturated with one atm of hydrogen gas at room temperature (17.7 scc kg^{-1}) will stabilize nickel metal at temperatures <309ºC, based on values for Henry's law constant calculated per Table 1. In other words, the solubility measurement at 316ºC in Runs 1, 2B, 4 and 5 was obtained in a region where NiO, rather than metallic nickel, was thermodynamically stable. To determine the extent to which measurements at other temperatures may have been affected, a more accurate method was devised to estimate the Gibbs energy change for Eq. (16).

Previous extrapolations to elevated temperature using Eq. (18, 19) were successful because the $C_P(T)$ curves for the reactants and products had similar shapes. This result occurs because

heat capacities are dominated by vibrational energies. Modeling of NiO becomes complicated at elevated temperatures, however, because NiO undergoes a magnetic ordering/disordering transition at 247ºC [17]: below 247ºC its crystalline lattice is configured in cubic symmetry, above 247ºC it reverts to rhombohedral symmetry. Metallic nickel exhibits similar behavior, except that its transition occurs at 357ºC [18]. These transitions create thermal anomalies in the heat capacity curves, such that the heat capacity curve for each solid decreases, rather than increases, as the critical temperature of water (~374ºC) is reached, see Fig. 7. Therefore, it is expected that the accuracy of Eq. (19) will be degraded when the equilibrium for Eq. (16) is calculated above 247ºC.

The above difficulty was overcome by allowing heat capacities of the solids to be expressed by the sum of a vibrational (baseline) and magnetic contribution. In the usual manner, the baseline contribution was fitted to a (constrained) five-parameter Maier-Kelley model:

$$C_P(T) = a + bT + cT^2 + d/T^2 + e/\sqrt{T} \qquad (20)$$

On the other hand, the magnetic contribution (i.e., λ-shaped transition) was fitted to a four-parameter Inden model [19] in dimensionless temperature ($\tau = T/T_C$):

$$C_P^{mag(-)} = 2K^- R\left[\tau^m + \frac{1}{3}\tau^{3m} + \frac{1}{5}\tau^{5m}\right] \qquad (\text{for } \tau < 1) \qquad (21)$$

$$C_P^{mag(+)} = 2K^+ R\left[\tau^{-n} + \frac{1}{3}\tau^{-3n} + \frac{1}{5}\tau^{-5n}\right]. \qquad (\text{for } \tau > 1) \qquad (22)$$

Although previous applications of the Inden model to the ferromagnetic transition in metals has found that m = 3 and n = 5 [20], these parameters were treated as adjustable in the values

reported in Table VII. Model parameters for NiO(s) and Ni(s) were obtained by least-squares fits of heat capacity data reported by Hemingway [17] and Meschter *et al*. [18], respectively. Heat capacities for liquid water at its saturation vapor pressure [21] were fitted to a modified form of Eq. (20), replacing the e$T^{-0.5}$ term by e'$(T - 647)^{-1}$. This substitution provided a correlation that is valid up to the critical temperature of water (T <647 K). All model parameters for Eq. (20) are tabulated in Table VII.

Extrapolations to elevated temperature were performed by applying the thermodynamic relationships

$$\Delta H^\circ(T) - \Delta H^\circ(298) = \int_{298}^{T} (\Delta C_P / T) dT \qquad (23)$$

$$= \Delta a T + (\Delta b/2) T^2 + (\Delta c/3) T^3 - \Delta d/T + 2\Delta e\sqrt{T} - e' \ln(647.27 - T)$$

and

$$\Delta S^\circ(T) - \Delta S^\circ(298) = \int_{298}^{T} (\Delta C_P / T) dT \qquad (24)$$

$$= \Delta a \ln T + \Delta b T + (\Delta c/2) T^2 - (\Delta d/2) T^{-2} - 2\Delta e/\sqrt{T} - (e'/647.27) \ln\left(\frac{647.27 - T}{T}\right)$$

The magnetic correction to Gibbs energy for NiO above 519 K was determined by the following integrations:

$$H^{mag}(T) = \int_{298}^{519} C_P^{mag(-)} dT + \int_{519}^{T} C_P^{mag(+)} dT \qquad (25)$$

$$S^{mag}(T) = \int_{298}^{519} \left(C_P^{mag(-)}/T\right) dT + \int_{519}^{T} \left(C_P^{mag(+)}/T\right) dT \qquad (26)$$

where $G^{mag}(T) = H^{mag}(T) - T\,S^{mag}(T)$. (27)

The magnetic correction for Ni metal is simpler because calculations were not performed above 633 K, so only $C_P^{mag(-)}$ integrations were required.

The resulting Gibbs energies for Eq. (16), obtained by applying Eqs. (23 - 27), are plotted in Fig. 8; the magnetic correction being shown along the bottom axis on an expanded scale. Also shown in Fig. 8 are the Gibbs energies for Eq. (16) calculated using the three parameter model, Eq. (19). Differences in Gibbs energies between the more rigorous model and the constant heat capacity model are seen to be insignificant (i.e., 0.1 kJ mol^{-1}) at temperatures up to about 580 K, but then increase to values as high as 0.5 kJ mol^{-1} at 630 K. Therefore, aqueous solutions in equilibrium with a one atmosphere blanket of hydrogen gas (at room temperature) are expected to oxidize nickel metal to NiO only at temperatures above 309ºC, essentially the same threshold as predicted using the previous, constant heat capacity model. This means that all of the present nickel metal solubility measurements recorded at 302ºC are indeed valid.

By way of closure, Fig. 9 compares the solubility behavior of metallic nickel and NiO in hydrothermal solutions whose alkalinity is typical of that maintained in commercial PWR coolants. This alkalinity, i.e., pH(at 300ºC) = 7.1, may be achieved by a sodium hydroxide solution having the concentration 0.078 mmol kg^{-1}. As expected, increases in hydrogen decrease Ni(II) ion solubility and stabilize Ni(s) relative to NiO(s). More importantly, however, the temperature dependency of each solubility curve at 300ºC is opposite: Ni(s) solubilities increase with temperature, while NiO(s) solubilities decrease with temperature. Therefore, boiling operations which tend to strip dissolved hydrogen from the coolant at the fuel surface, can stabilize NiO 'crud' deposits, relative to Ni(s), and lead to further buildup of NiO on the heated fuel surfaces due to its inverse temperature solubility curve.

SUMMARY AND CONCLUSIONS

A platinum-lined, flowing autoclave facility was used to investigate the solubility behavior of metallic nickel in hydrogenated ammonium and sodium hydroxide solutions between 175 and 315ºC at a system pressure of 13.1 MPa. Ni(II) ion solubilities were found to range between 0.6 nmol kg^{-1} (the minimum reportable value for the analytical methodology employed herein) and 8.5 nmol kg^{-1}. Based on the accumulated solubility database and the subsequent thermodynamic analyses afforded the data, it is concluded that:

1. Metallic nickel solubilizes in hydrogenated hydrothermal environments by undergoing an oxidative dissolution reaction:

$$Ni(s) + 2H^{+}(aq) = Ni^{2+}(aq) + H_2(g) \quad (1)$$

2. Nickel(II) ion solubilities are enhanced by the formation of two Ni(II) ion hydrolysis products which were characterized by the following chemical reactions:

$$Ni^{2+}(aq) + nH_2O = Ni(OH)_n^{2-n}(aq) + nH^{+}(aq) \quad (2)$$

where n = 1, 2.

3. A set of thermochemical properties ($\Delta_f G^{\circ}$, $\Delta_f H^{\circ}$, S°) was extracted for $Ni^{2+}(aq)$, $Ni(OH)^{+}(aq)$ and $Ni(OH)_2(aq)$ from the equilibria determined for Eqs. (1, 2) by non-linear regression analyses. Thermodynamic consistency with accepted literature properties (at room temperature) was achieved by constraining $\Delta G^{\circ}(298)$ for Eq. (2), n = 2, by applying previously determined standard Gibbs energies for each of the chemical entities in Eq. (2), n = 2 [3]. Ni(II) ion amminocomplexes were found to be negligible.

4. The above properties are internally consistent with those obtained previously in our laboratory during a solubility study of $NiO/Ni(OH)_2$ over the temperature range 25 – 315ºC.

5. The present levels of temperature and dissolved hydrogen were shown to stabilize nickel metal relative to nickel(II) oxide, except at the lowest hydrogen level (17.7 scc kg^{-1}) and highest temperature (315ºC) tested. Although this result is consistent with estimates based on known thermodynamic properties of NiO and Ni, which predict a Ni/NiO transformation temperature at 309ºC for this level of dissolved hydrogen, the predicted Ni/NiO phase boundary remains in disagreement with independent measurements obtained using a thin-walled Pd-Ag cell [4, 23].

REFERENCES

[1] J. A. Gorman, J. E. Harris, R. W. Staehle, K. Fruzzetti, Secondary side corrosion of 600MA tubing in PWR steam generators – Causes, implications for Alloys 600TT and 690TT, and needed research, in *Proceedings 11th International Conference on Environmental Degradation of Materials in Nuclear Systems – Water Reactors,* G. S. Was and L. Nelson eds., American Nuclear Society (2003), 362-79

[2] F. Nordmann, Efficient, sustainable and economical plant operation, in *Proceedings International Conference on Water Chemistry of Nuclear Reactor Systems, 2006*, Jeju Island, Korea (2006), paper 1.2

[3] S. E. Ziemniak, M. A. Goyette, Nickel(II) oxide solubility and phase stability in high temperature aqueous solutions, J. Solution Chem. 33 (2004) 1135-59

[4] S. A. Attanasio, D. S. Morton, Measurement of the nickel/nickel oxide transition in NiCrFe alloys and updated data and correlations to quantify the effect of aqueous hydrogen on primary water SCC, in *Proceedings 11th International Conference on Environmental Degradation of Materials in Nuclear Systems – Water Reactors,* G. S. Was and L. Nelson eds., American Nuclear Society (2003), 144-55

[5] S. E. Ziemniak, M. Hanson, Corrosion behavior of NiCrFe Alloy 600 in high temperature, hydrogenated water, Corrosion Sci. 48 (2006) 498-521

[6] L. O. Gilpatrick, H. H. Stone, *Oak Ridge National Laboratory Reports* ORNL-3127 (1961) and ORNL-3262 (1962)

[7] R. Fernandez-Prini, R. Crovetto, Evaluation of data on solubility of simple apolar gases in light and heavy water at high temperature, J. Phys. Chem. Ref. Data 18 (1989) 1231-43

[8] F. H. Sweeton, R. E. Mesmer, C. F. Baes, Acidity measurements at elevated temperatures. VII. Dissociation of water, J. Solution Chem. 3 (1974) 191-214

[9] B. F. Hitch, R. E. Mesmer, The ionization of aqueous ammonia to 300ºC in KCl media, J. Solution Chem. 5 (1976) 667-80

[10] W. L. Marshall, R. Slusher, E. V. Jones, Aqueous systems at high temperature. XIV. Solubility and thermodynamic relation for $CaSO_4$ in NaCl-H_2O solutions from 40º to 200º, 0 to 4 m NaCl, J. Chem. Eng. Data 9 (1964) 187-91

[11] W. L. Marshall, E. V. Jones, Second dissociation constant of sulfuric acid from 25 to 350º evaluated from solubilities of calcium sulfate in sulfuric acid solutions, J. Phys. Chem. 70 (1966) 4028-40

[12] D. D. Wagman, W. H. Evans, V. B. Parker, R. H. Schumm, I. Halow, S. M. Bailey, K. L. Churney, R. L. Nuttall, The NBS tables of chemical thermodynamic properties, J. Phys. Chem. Ref. Data 11 (1982) Suppl. 2

[13] D. L. Marquardt, An algorithm for least-squares estimation of nonlinear parameters, J. Soc. Indust. Appl. Math. 2 (1963) 431-41

[14] R. E. Mesmer, W. L. Marshall, D. A. Palmer, J. M. Simonson, H. F. Holmes, Thermodynamics of aqueous association and ionization reactions at high temperatures and pressures, J. Solution Chem. 21 (1988) 699-718

[15] D. J. Wesolowski, S. E. Ziemniak, L. M. Anovitz, M. L. Machesky, P. Benezeth and D. A. Palmer, Solubility and surface adsorption characteristics of metal oxides, in *Aqueous Systems at Elevated Temperatures and Pressures,* D. A. Palmer, R. Fernandez-Prini and A. H. Harvey eds., Elsevier, New York (2004), Ch. 14

[16] P. R. Tremaine and J. C. LeBlanc, The solubility of nickel oxide and hydrolysis of Ni^{2+} in water to 573 K, J. Chem. Thermodyn. 12 (1980) 521-38

[17] B. S. Hemingway, Thermodynamic properties for bunsenite, NiO, magnetite, Fe_3O_4, and hematite, Fe_2O_3, with comments on selected oxygen buffer reactions, Am. Mineral. 75 (1990) 781-90

[18] P. J. Meschter, J. W. Wright, C. R. Brooks, T. G. Kollie, Physical contributions to the heat capacity of nickel, J. Phys. Chem. Solids 42 (1981) 861-71

[19] D. de Fontaine, S. G. Fries, G. Inden, P. Miodownik, R. Schmid-Fetzer, S.-L. Chen, Thermodynamic models and data for pure elements and other end members of solutions, Calphad 19 (1995) 499-536

[20] A. T. Dinsdale, SGTE data for pure elements, Calphad 15 (1991) 317-425

[21] W. T. Parry, J. C. Bellows, J. S. Gallagher and A. H. Harvey, *ASME International Steam Tables for Industrial Use,* CRTD-Vol. 58, ASME Press, New York (2000)

[22] K. K. Kelley, Critical evaluation of high-temperature heat capacities of inorganic compounds, U. S. Bur. Mines, Bull. No. 476 (1949)

[23] D. H. Lee, M. S. Choi and U. C. Kim, Effect of hydrogen and Li/B concentration on the stress corrosion cracking of Alloy 600 in simulated PWR primary water at 330ºC, in *Proceedings International Conference on Water Chemistry of Nuclear Reactor Systems, 2006*, Jeju Island, Korea (2006), paper 2.7

TABLE I

Feedwater Chemistry

Run No.	Ammonia, mmol-kg^{-1}	pH @ 25ºC	Conductivity :S-cm^{-1}	P_{H2} atm
1	0.147±0.005	9.53±0.01	11.6±0.5	1.06±0.02
2A	0.150	9.52	11.4	3.27
2B	0.164	9.53±0.05	11.7±0.3	1.07±0.02
3	0.687±0.019	10.01±0.02	25.9±1.5	3.07±0.03
4*	0.608±0.056	9.87±0.03	24.1±1.2	1.05±0.02
5	1.458±0.073	10.14±0.03	41.4±1.2	1.05±0.02
6	5.67±0.49	10.44±0.03	80.8±1.4	4.01±0.23
	NaOH, mmol-kg^{-1}			
7	0.061±0.002	9.62±0.06	11.4±0.9	3.93±0.08
8	0.181±0.007	10.19±0.03	35.7±3.1	4.01

*Double run

TABLE II

Calculations for ICPMS Calibration Curve

Ni Conc. Increase From Stock Solution, ppt*	Dilution Factor	ICPMS Signal Counts/sec	Recalc. Ni Conc. ppt
2196	0.455×10^6	6100	2220
1256	0.796×10^6	3550	1280
625	1.600×10^6	1800	645
342	2.923×10^6	996	362
155	6.452×10^6	484	175
Blank	--	32.8	20

* Neglects presence of nickel in ultrapure water.

TABLE III

Solubilities of Ni Metal in Hydrogenated Aqueous Solutions

Run 1		Run 2B		Run 2A		Run 4U		Run 4D	
Ni, nm	Temp, K	Ni, nm	Temp, K	Ni, nm	Temp, K	Ni, nm	Temp, K	Ni, nm	Temp, K
4.26	449.8	3.56	449.8	1.46	449.8	1.53	449.8	1.91	449.8
4.79	463.7	3.42	463.7	1.74	463.7	1.70	463.7	2.20	463.7
5.26	477.6	4.34	477.6	1.35	477.6	1.77	477.6	2.33	477.6
5.76	491.5	4.17	491.5	1.69	491.5	2.32	491.5	2.49	491.5
6.40	505.4	5.16	505.4	1.48	505.4	2.64	505.4	2.81	505.4
6.98	519.3	5.20	519.3	2.06	519.3	2.59	519.3	3.07	519.3
7.10	533.5	5.60	533.5	1.64	533.5	3.00	533.5	3.12	533.5
6.73	547.0	--	547.0	2.10	547.0	3.17	547.0	3.30	547.0
6.73	560.9	5.48	560.9	1.75	560.9	3.24	560.9	3.29	560.9
6.93	574.8	5.23	574.8	2.64	574.8	3.29	574.8	3.32	574.8
(8.01)	588.7	(5.33)	588.7	1.69	588.7	(2.76)	588.7	(2.76)	588.7

Parentheses denote potential non-equilibrium data.

TABLE III (Cont'd)

Solubilities of Ni Metal in Hydrogenated Aqueous Solutions

Run 3		Run 5		Run 6		Run 7		Run 8	
Ni, nm	Temp, K	Ni, nm	Temp, K	Ni, nm	Temp, K	Ni, nm	Temp, K	Ni, nm	Temp, K
<mr	449.8	0.92	449.8	<mr	449.8	<mr	449.8	<mr	449.8
<mr	463.7	0.78	463.7	<mr	463.7	<mr	463.7	<mr	463.7
<mr	477.6	0.77	477.6	<mr	477.6	<mr	477.6	<mr	477.6
1.00	491.5	0.99	491.5	<mr	491.5	<mr	491.5	--	491.5
0.94	505.4	0.77	505.4	<mr	505.4	<mr	505.4	<mr	505.4
0.99	519.3	1.12	519.3	<mr	519.3	--	519.3	<mr	519.3
1.18	533.5	0.94	533.5	<mr	533.5	<mr	533.5	<mr	533.5
1.06	547.0	1.23	547.0	0.83	547.0	0.49	547.0	<mr	547.0
1.29	560.9	2.14	560.9	<mr	560.9	--	560.9	<mr	560.9
1.06	574.8	1.37	574.8	0.89	574.8	0.49	574.8	0.66	574.8
1.04	588.7	(1.16)	588.7	<mr	588.7	0.73	588.7	<mr	588.7

Minimum reportable values (mr): 0.85 nm (Run 3), 0.77 nm (Run 6) and 0.50-0.77 nm (Runs 7 & 8).

Parentheses denote potential non-equilibrium data.

TABLE IV

Ionization Behavior of Selected Compounds *via* Eq. (6)

Compound Undergoing Ionization	b_1	b_2	b_3	b_4	b_5	Reference Cited
H_2O	31,286.0	-606.522	94.9734	-0.097611	-2,170,870	Sweeton *et al.* [8]
NH_4OH	27,496.7	-513.761	81.2824	-0.0905795	-1,717,720	Hitch and Mesmer [9]
H_2[a]	27,416.5	-449.429	70.6703	-0.0655463	-1,848,130	Gilpatrick and Stone [6]

[a] Henry's law

TABLE V

Thermodynamic Parameters Fitted for the Calculation of Nickel Metal Solubility Behavior in Hydrogenated Sodium and Ammonium Hydroxide Solutions*

Reaction	$\Delta H^{\circ}(298)$ kJ-mol^{-1}	$\Delta S^{\circ}(298)$ J-mol^{-1}-K^{-1}	$\Delta G^{\circ}(298)$ kJ-mol^{-1}
$Ni(s) + 2H^{+} = Ni^{2+}(aq) + H_2(g)$	-70.34±13.35	-68.36±27.12	-49.95±5.31
$Ni(s) + H^{+} + H_2O = Ni(OH)^{+} + H_2(g)$	-47.66±10.11	-145.03±20.75	-4.42±3.96
$Ni(s) + 2H_2O = Ni(OH)_2(aq) + H_2(g)$	61.92±0.73	-77.83	85.13**

* $\log K = -\Delta G^{\circ}/RT$, where $\Delta G^{\circ} = \Delta H^{\circ} - T\Delta S^{\circ}$.

** Constrained value per Table VI in Ref. [3].

TABLE VI

Comparison of Thermochemical Properties of Ni(II) Ion Aquohydroxocomplexes Derived from Solubility Studies of Ni Metal, Ni(II) Oxide and Ni(II) Hydroxide

Species	$S°(298)$ J-mol^{-1}-K^{-1}	$\Delta_f H°(298)$ kJ-mol^{-1}	$\Delta_f G°(298)$ kJ-mol^{-1}	Reference
$Ni^{2+}(aq)$	-213.6±27.1	-70.34±13.35	-49.95±5.31	This work
	-172.5±5.6	-52.42±2.64	-44.28	Ziemniak & Goyette [3]
	-176.7	-52.75	-43.36	Tremaine & LeBlanc [16]
	-264.7	-73.22	-37.59	Palmer *et al.* [15]
$Ni(OH)^{+}(aq)$	-198.1±20.8	-333.49±10.11	-241.56±3.96	This work
	-135.6±5.7	-300.82±2.24	-227.53	Ziemniak & Goyette [3]
	-72.2	-266.36	-211.96	Tremaine & LeBlanc [16]
$Ni(OH)_2(aq)$	-38.8	-509.74±0.73	-389.15*	This work
	-45.1±13.2	-511.62±7.05	-389.15	Ziemniak & Goyette [3]
	-65.2	-530.48	-402.01	Tremaine & LeBlanc [16]
	-43.2	-521.43	-399.53	Palmer *et al.* [15]

* Value constrained for consistency with Ref. [3].

TABLE VII

Temperature Functionality of Heat Capacity
for Compounds Involved in Ni/NiO Phase Boundary *via* Eq. (20)

Compound	a	b	c	d	e	Range
Ni(s)*	37.897	$-8.762\ 10^{-3}$	$6.857\ 10^{-6}$	$-4.019\ 10^{5}$	-86.154	250-1700 K
Eqs. (21,22) (Inden)	T_C = 633 K	m = 11.126 ± 1.390 n = 29.424 ± 10.315		$2RK^- = 6.397 \pm 0.246$ $2RK^+ = 2.679 \pm 0.317$		
NiO(s)*	64.181	$-1.254\ 10^{-2}$	$6.822\ 10^{-6}$	$-1.375\ 10^{6}$	-32.785	338-1800 K
Eqs. (21,22) (Inden)	T_C = 519 K	m = 4.869 ± 0.220 n = 12.041 ± 0.697		$2RK^- = 10.792 \pm 0.116$ $2RK^+ = 7.288 \pm 0.148$		
H_2(g)**	27.280	$3.2635\ 10^{-3}$	0	$5.0208\ 10^{4}$	0	298-3000 K
H_2O	94.018	$-1.12488\ 10^{-1}$	$1.13434\ 10^{-4}$	$-2.79331\ 10^{5}$	-2779.10***	T<647 K

* Parameters in Maier-Kelley correlation, Eq. (20), were constrained to provide limiting C_P values for Ni(s) = 40.59 J mol^{-1} K^{-1} at 1700 K and NiO(s) = 62.52 J mol^{-1} K^{-1} at 1800 K. ** Parameters taken from Ref. [22]. *** $e/T^{0.5}$ term replaced by $e'/(T-647)$.

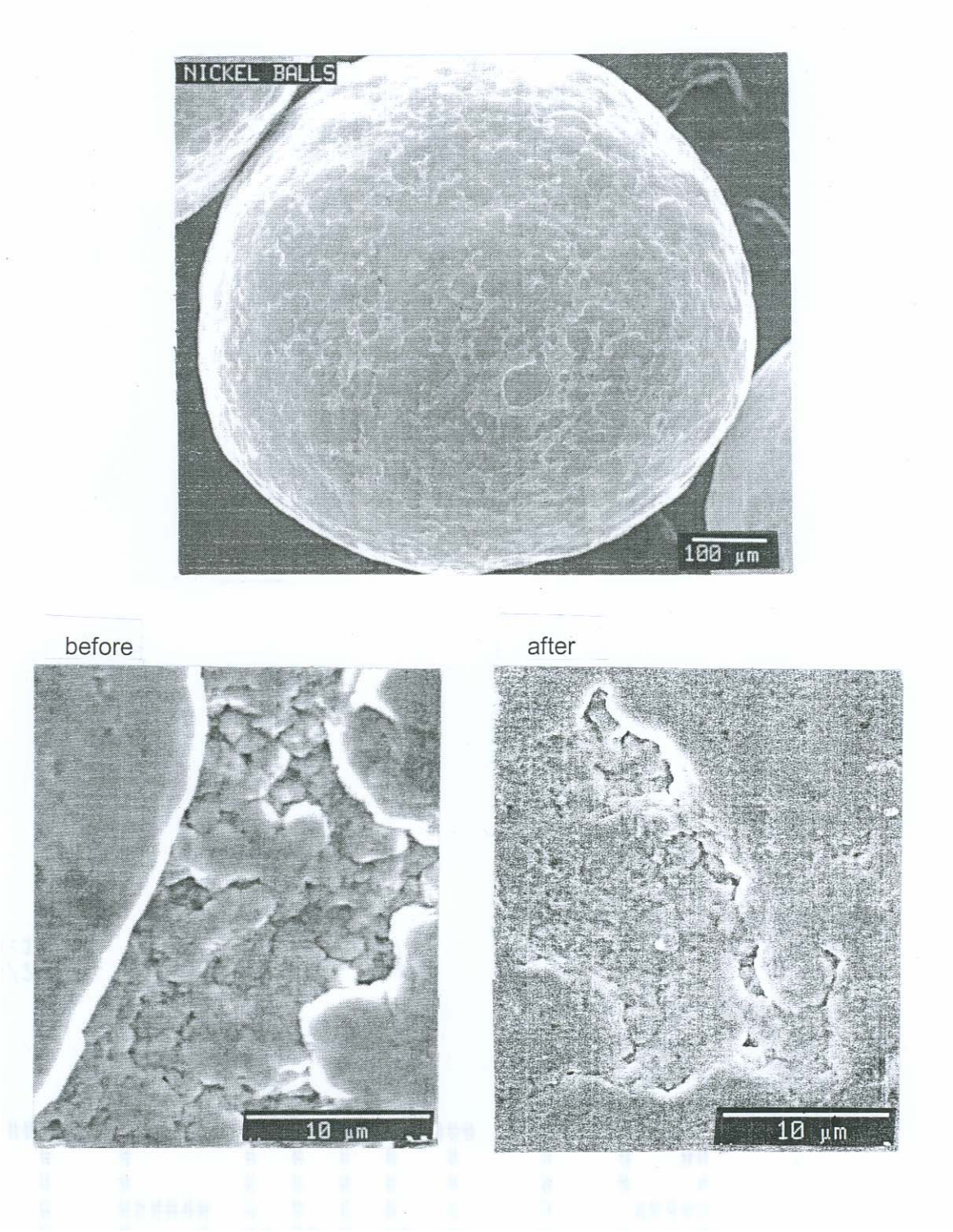

Fig. 1. SEM images of nickel spheres used in solubility study. Smooth regions correspond to areas plasticly-deformed during the sphere-shaping operation.

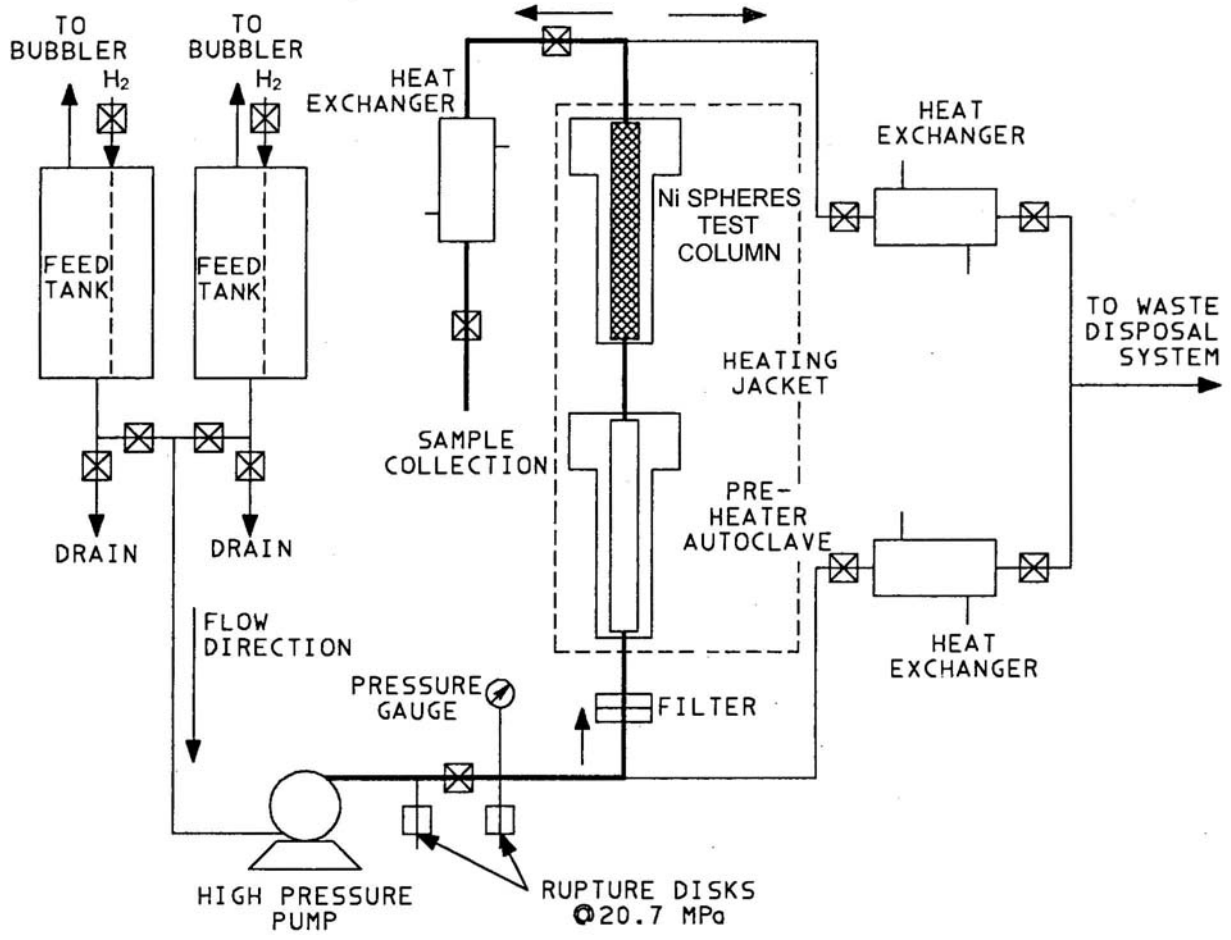

Fig. 2. Schematic of flowing autoclave system used in solubility investigation of metallic nickel mini-spheres.

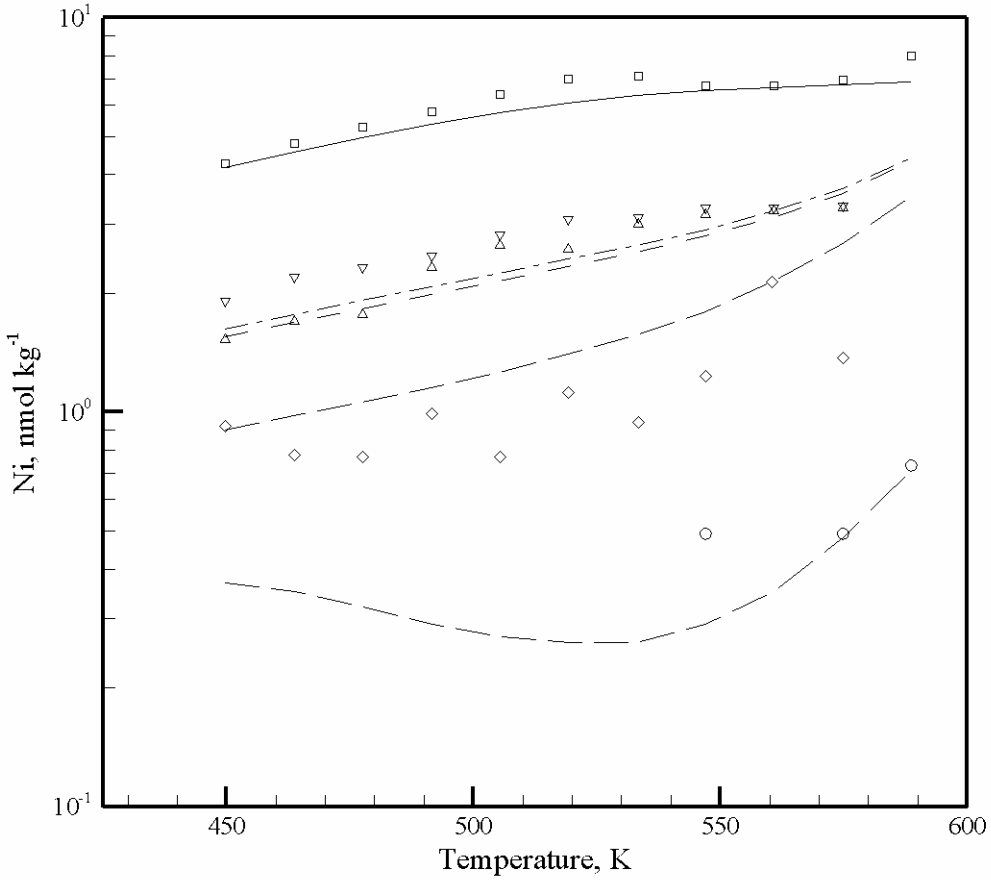

Fig. 3. Comparison of measured and fitted solubilities of nickel metal in hydrogenated aqueous solutions: □ Run 1 ▼ Run 4 (up), Δ Run 4 (down), ♦ Run 5 and ○ Run 7. mr = 0.50 nmol kg^{-1} for Run 7.

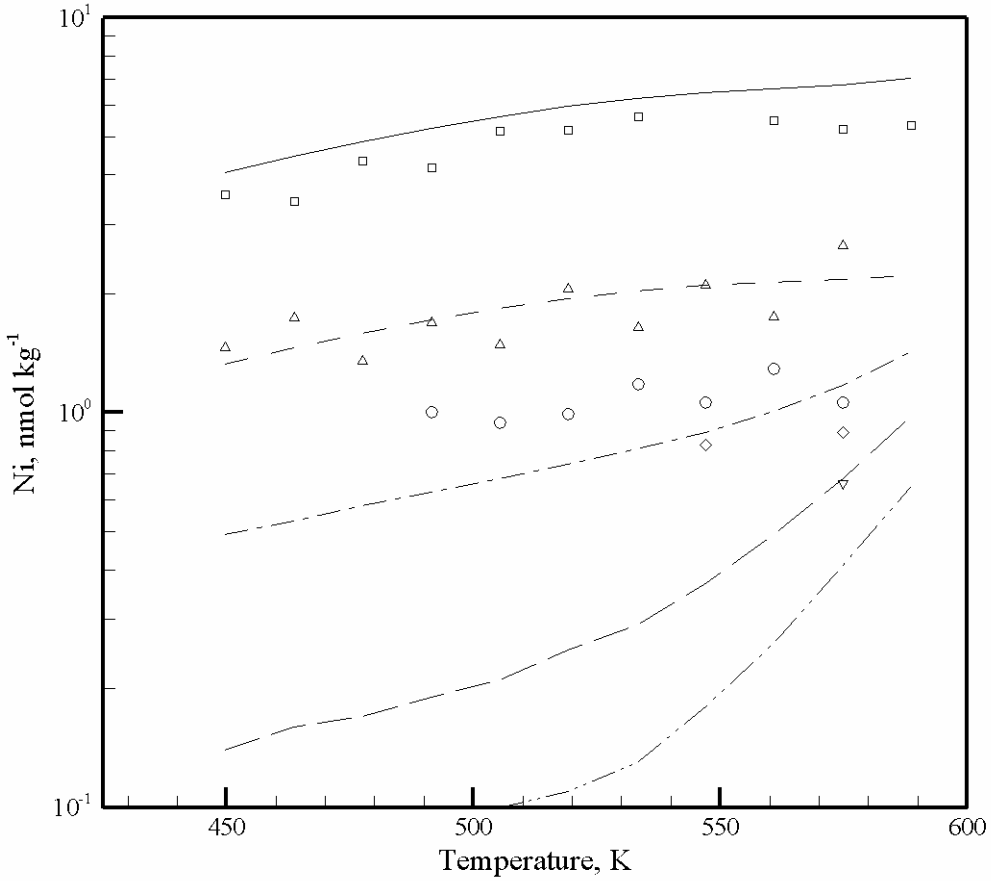

Fig. 4. Comparison of measured and fitted solubilities of nickel metal in hydrogenated aqueous solutions: □ Run 2B, Δ Run 2A, ○ Run 3, ♦ Run 6 and ▼ Run 8. mr = 0.85 nmol kg^{-1} for Run 3; mr = 0.60 nmol kg^{-1} for Runs 6 and 8.

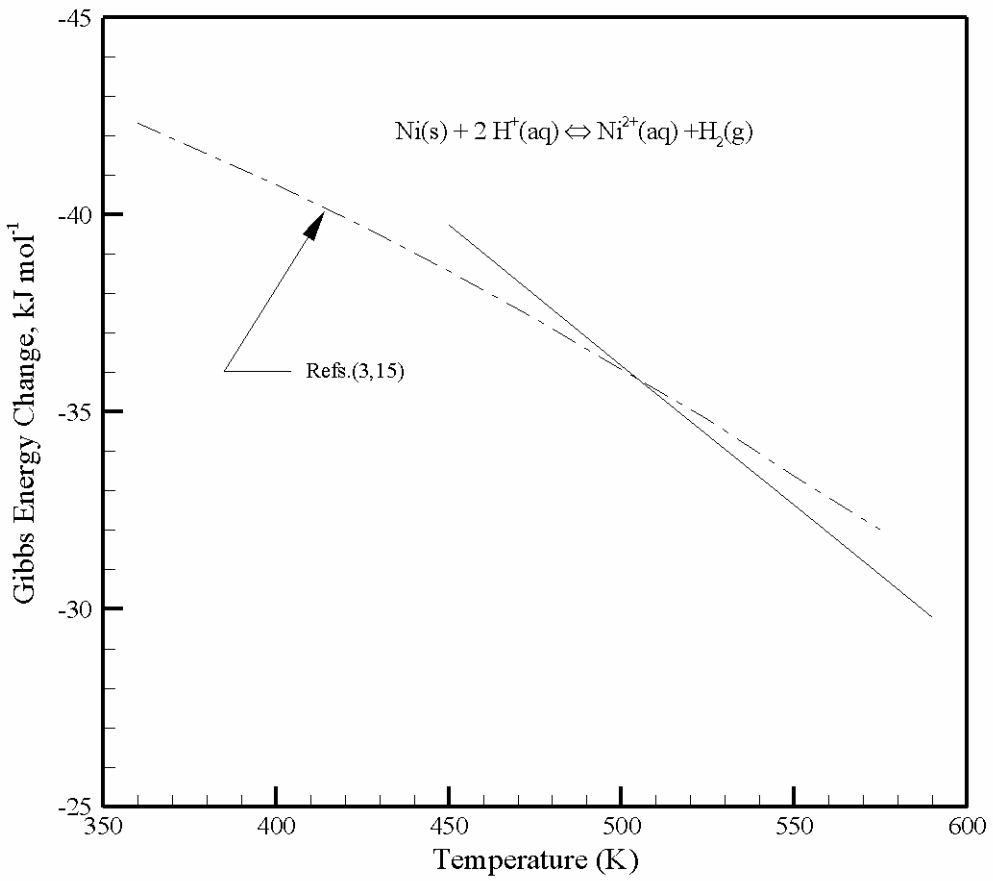

Fig. 5. Gibbs energy changes for the oxidative dissolution of metallic nickel in aqueous solutions.

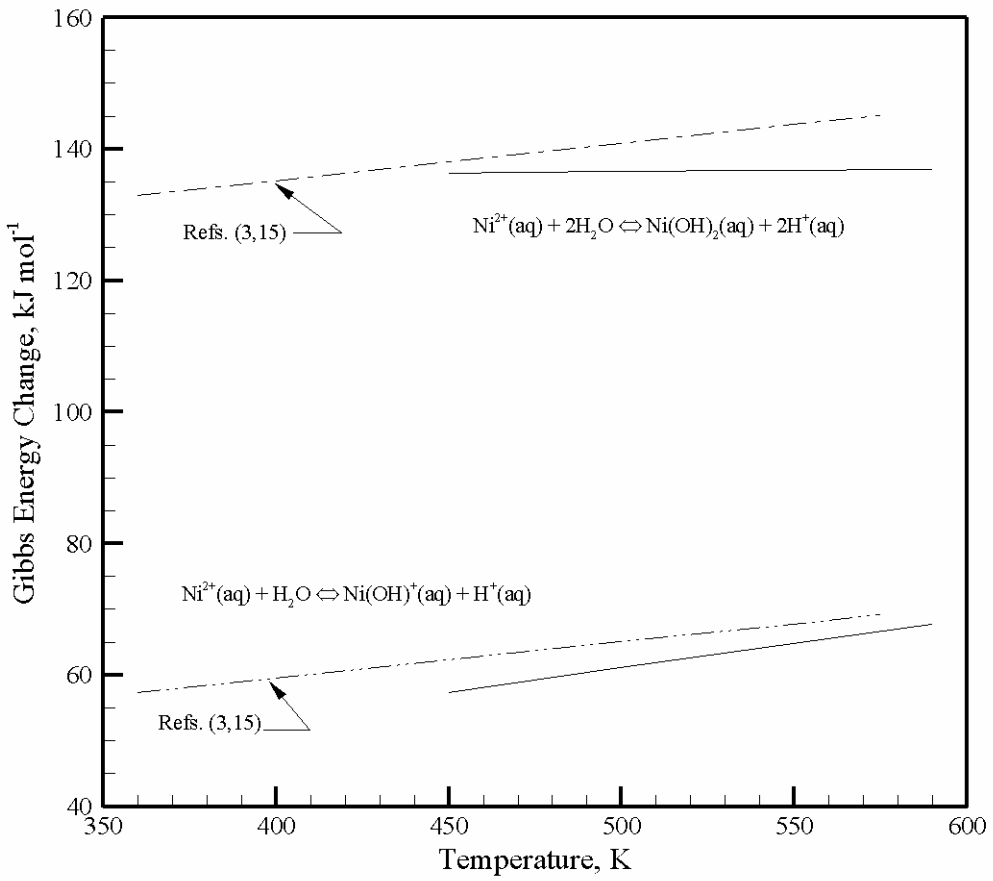

Fig. 6. Gibbs energy changes for the first two hydrolysis reactions of the Ni(II) aquoion.

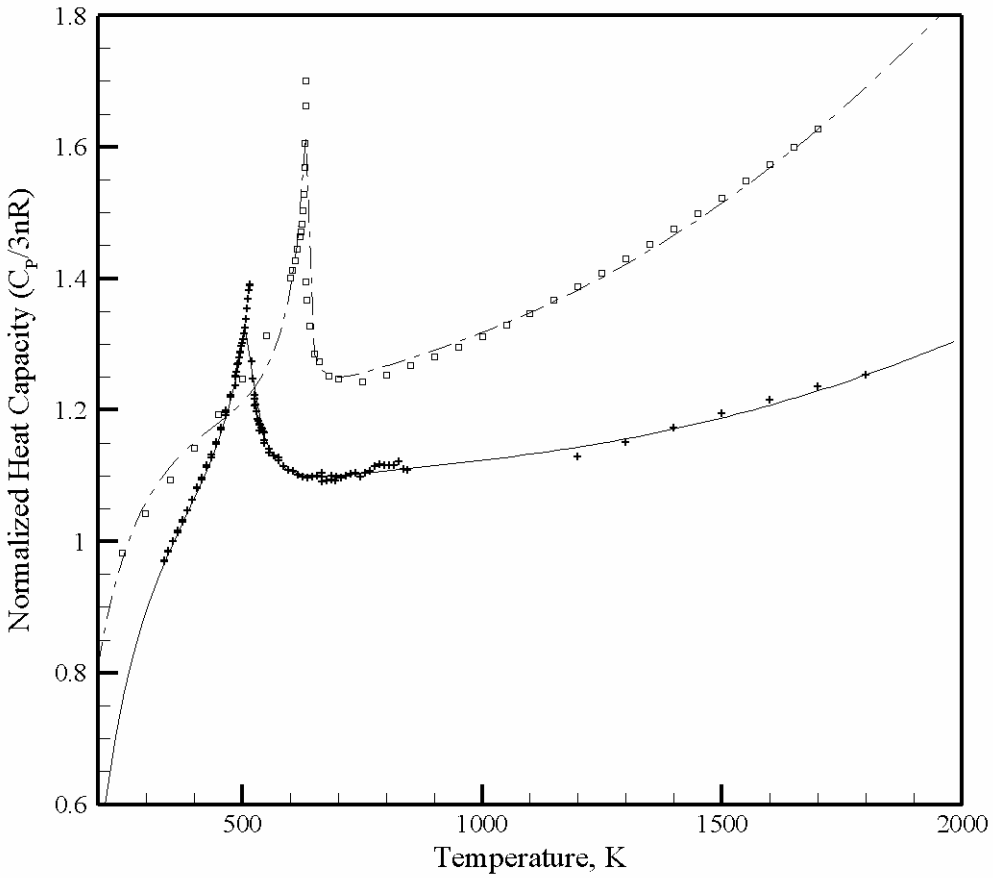

Fig. 7. Normalized heat capacities (C_P/3nR) of nickel metal (upper, n = 1) and nickel(II) oxide (lower, n = 2). Data for NiO and Ni taken from Hemingway [17] and Meschter *et al*. [18], respectively.

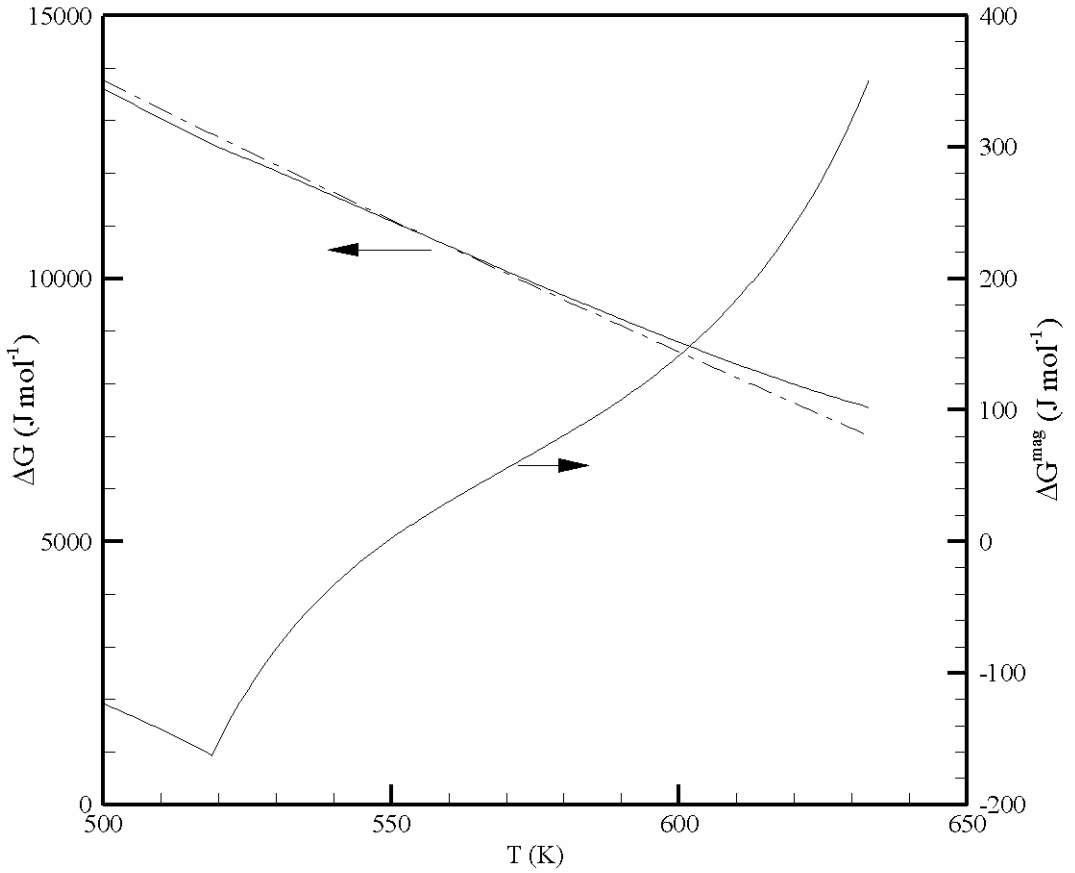

Fig. 8. Ni/NiO phase boundary in aqueous solutions: (a) three parameter model, Eq. (19) (dashed line) and (b) allowance for thermal anomalies due to magnetic transitions, per Table VI (solid line). Magnetic correction to Gibbs energy for Eq. (16) shown at bottom of figure on an expanded scale.

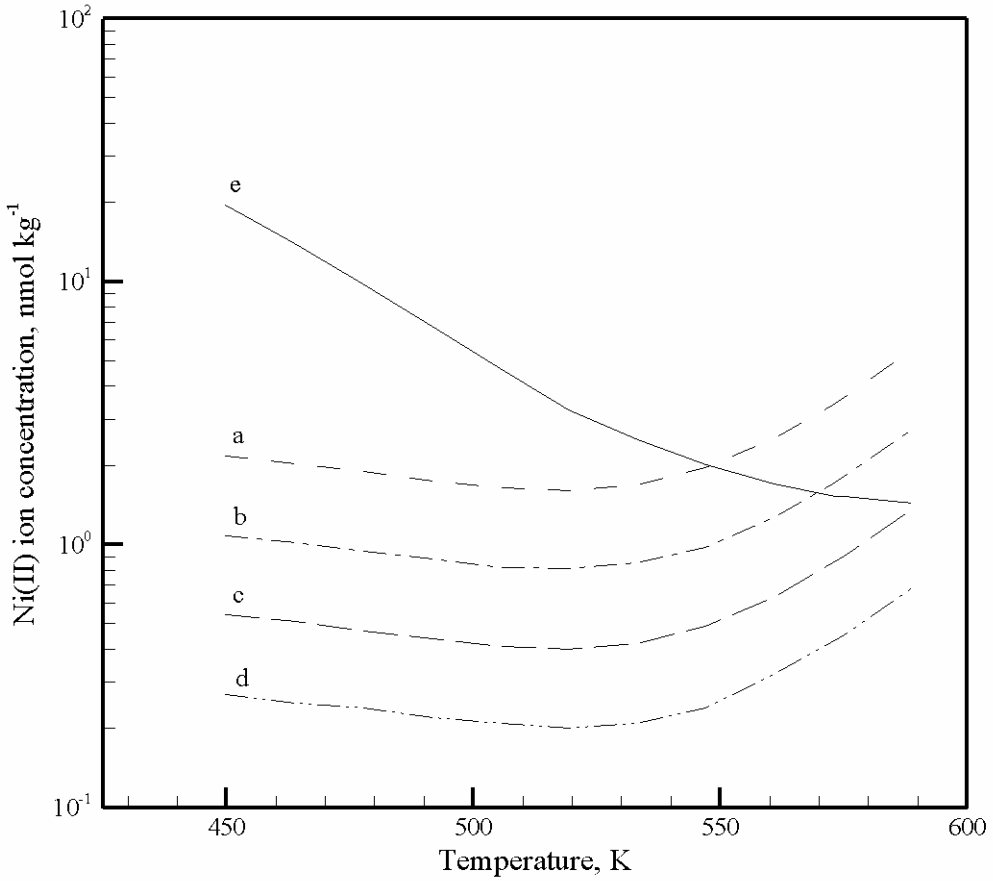

Fig. 9. Effects of temperature and dissolved hydrogen on Ni(II) ion solubility in a dilute sodium hydroxide solution (0.078 mmol kg^{-1}). Solubility of metallic nickel plotted for dissolved hydrogen levels: (a) 8.85 scc kg^{-1}, (b) 17.7 scc kg^{-1}, (c) 35.4 scc kg^{-1} and (d) 70.8 scc kg^{-1}; (e) solubility of NiO(s) taken from Ref. [3]. Note: solubility of NiO is independent of hydrogen level; equivalence of Ni(II) ion solubility indicates Ni/NiO phase boundary.